Neuron, volume *76*

Supplemental Information

Correlated Variability in Laminar Cortical Circuits

Bryan J. Hansen, Mircea I. Chelaru, and Valentin Dragoi

Inventory of Supplemental Information

Supplementary Methods (electrophysiological recordings)

Multi–contact electrophysiological recordings

Single–unit recordings were amplified, filtered, and viewed on an oscilloscope and heard through a speaker. The spike waveforms where sorted using Plexon's offline sorter program that implemented waveform clustering based on parameters such as principal components (**Figure 1**C), spike width, valley and peak. When a unit was isolated, its receptive field was mapped using a reverse correlation stimulus, while the animal maintained fixation. Receptive fields across contacts are mapped using stimuli presented in random patches on a computer screen consisting of oriented gratings at 0, 45, 90 and 135°. Firing rates for each neuron are calculated independently at 5 ms intervals between 40 to 120 ms at each spatial location. After the maximum firing rates (identified as red) are calculated, we computed the centroid for each time delay. For each cell, the time delay with the minimum distance between the centroid and adjacent firing rate locations was chosen to determine the shape of the receptive field. Recording sites were selected on the basis of the quality of the signal (signal–to–noise ratio) and their receptive field position. Using home–made scripts in MATLAB and Plexon's Offline Sorter we analyzed the unit's waveform characteristic (i.e. width and peak), firing rate, and orientation selectivity. Single–units which abruptly changed their responses (i.e. increases or decreases in firing rate and/or changes in orientation selectivity) were removed and only those units with stable firing rate and orientation selectivity were kept for further analysis.

LFP analysis

LFPs were filtered using high–pass and low–pass equiripple finite impulse response (FIR) filters with cutoff frequencies of 0.5 Hz and 100 Hz respectively with 60 dB stopband attenuations. In order to remove line artifacts, we applied a digital notch at 60 Hz (4^{th} order elliptic filter, 0.1 db peak–to–peak ripples, 40 dB stopband attenuation; the cross–correlation between the monitor 60 Hz refresh pulses and spikes and LFPs for our entire population failed to find a signature of locking). All filtering was applied by using forward and backwards filtering to obtain zero phase shifts. To correct for the time delays induced in the LFP signals by the filters in headstages and pre–amplification boards we used the software correction FPAlign provided by Plexon (http://www.plexon.com/downloads.html). We discarded all LFPs that had more than 3 points outside the mean ± 4 standard deviations to avoid influence of experimental noise or movement artifact.

Current source density (CSD) analysis

For each recording session, we verified the laminar position of the electrode contacts by computing the evoked potential (ERP) profiles for brief visual stimulation during a passive fixation task. Briefly, monkeys were exposed to a full–field black screen that flashed white for 100 ms, and then returned to black. The LFP responses recorded with the laminar probe were processed to obtain ERP traces for each contact (ERPs were recorded for 100 trials). Indeed, Schroeder and colleagues have previously combined laminar recording, microlesion, and histological reconstruction to validate the effectiveness of the ERP method in the functional identification of cortical layers in V1. We computed the CSD, by using the 2^{nd} spatial derivative of the LFP time–series across equally–spaced laminar contacts using the iCSD toolbox for MATLAB (http://software.incf.org/software/csdplotter/home; Pettersen et al., 2006). This analysis allowed us to accurately identify the polarity inversion accompanied by the sink–source

configuration at the base of L4 (the sink is inside L4). Using home–made MATLAB programs we analyzed the laminar CSD profile to verify the presence of a primary sink in the granular layer in each of the 34 recording sessions. This was accomplished by locating the sink driven negative polarity in the CSD plot, and then computing the center–of–mass of the granular sink. We obtained a single coordinate from this analysis consisting of the contact number and the time (in ms) when the sink was largest (centroid). The contact with the sink centroid served as the granular layer reference at 0 μm. We then analyzed all the contacts above and below the reference and grouped them (based on their sink/source waveform characteristics, cf. **Figure 1**B CSD traces) into one of three possible layers: supragranular, granular, and infragranular. Several controls were performed to test the reliability of our measure in identifying cortical layers: (i) we observed that micron advancement of the laminar electrode was highly correlated with a corresponding shift in the center–of–mass of the granular sink ($r = 0.89$, $P < 0.001$, Pearson's Correlation), (ii) shuffling electrode contacts as a function of cortical depth destroyed the laminar CSD profile (Hansen et al., 2011) and, (iii) vertical penetrations across all layers revealed a columnar organization based on the orientation preference of the spike responses.

Eye Movements

Eye position was continuously monitored using an eye tracker system (EyeLink II, SR Research Ltd., Osgoode, ON, Canada) with a binocular 1 kHz sampling rate. Eye position was calibrated before each experiment using a 5–point calibration procedure in which the animal was required to fixate on each one of 5 points (1 in the center, 2 in the vertical, and 2 in the horizontal axes or the diagonals) in steps of 4°, 8°, and 12° from the central fixation spot. The eye–tracker gains were adjusted such as to be linear for the horizontal and vertical eye deflections. The fixation pattern was analyzed to rule out any systematic bias and inconsistency during fixation. Microsaccades were analyzed every 10 ms by using a vector velocity threshold of 10°/s (this corresponds to a 0.1° eye movement between consecutive 10 ms intervals). Given our relatively high correlations it is possible that our results may be partially contaminated by fixational eye movements. We first explored trial–to–trial changes in amplitude according the formula:

$$\sqrt{(x_1 - x_2)^2 + (y_1 - y_2)^2} \qquad (1)$$

where x and y represent the position of the eye on the computer screen. We examined how the amplitude and velocity of microsaccades affect noise correlations in each cortical layer. For a given session, we computed the amplitude and velocity of eye movements (x and y) during the entire stimulus presentation (300 ms) on a trial–to–trial basis. We rank ordered each trial from smallest change in amplitude (i.e. no change in x and y eye position) to largest change in amplitude. We then identified the 1st quartile of the trials containing the largest change in amplitude. We further extended this analysis to include both the 1st and 2nd quartiles, which is equivalent to dividing the data into small vs. large eye movement trials. Not surprisingly, we observed a significant overlap between trials with large changes in eye movement amplitude and velocity (~ 85.2%). While removing trials with both large amplitude and high velocity eye movements reduced somewhat the number of trials used in our calculation of noise correlations, our main result remained unchanged, i.e., noise correlations were reduced but their laminar dependence was preserved (**Figure S3**; average of all 327 pairs; 1st quartile: one–way ANOVA, $F(2, 324) = 16.13$, $P = 10^{-7}$; 1st and 2nd quartile: one–way ANOVA, $F(2, 324) = 7.45$, $P = 0.0007$; post–hoc multi–comparison, Tukey's Least Significant Difference).

Noise correlations

We examined the laminar dependence of fluctuations in neuronal responses, or "noise", and measured spike count correlations (r_{SC}) between pairs of neurons in different layers. Noise correlations represent the Pearson correlation in trial–to–trial responses of spike counts between a pair of neurons for multiple presentations of an identical stimulus. The calculation of r_{SC} for a pair of neurons responding to particular stimulus orientation (θ) is as follows:

$$r_{sc}(\theta) = \frac{\sum_{k=1}^{N}(r_{ik} - r_i)(r_{jk} - r_j)}{N\sigma_i\sigma_j} = \frac{\sum_{k=1}^{N} r_{ik}r_{jk} - r_i r_j}{N\sigma_i\sigma_j} \quad (2)$$

where N is the number of trials, r_{ik} is the firing rate of neuron i in trial k, r_i is the mean firing rate, and σ_i is the standard deviation (STD) of the responses for neuron i (Bair et al., 2001). Given that we presented a range of stimuli, we had to aggregate noise correlations corresponding to different orientations. We did this by transforming the firing rates of neurons into z-scores, $r_{ik} \rightarrow z_{ik} = (r_{ik} - r_i)/\sigma_i$. Dividing the firing rates by the STD eliminates the effect that stimulus orientation has on the computation of noise correlation. Since all the z-score sequences have a zero mean and STD = 1, the noise correlation for one orientation θ (Eq. 2) is $r_{sc}(\theta) = E(z_{ik}(\theta)z_{jk}(\theta))$. In order to compute the noise correlation for all the stimulus orientations $\{\theta_1, \theta_2,..., \theta_n\}$, we computed, for each neuronal pair, the correlations $r_{sc}(\theta_1)$, $r_{sc}(\theta_2)$,...$r_{sc}(\theta_n)$ and then averaged them in order to obtain the noise correlation coefficient for that pair:

$$r_{SC} = E[r_{sc}(\theta_1), r_{sc}(\theta_2),..., r_{sc}(\theta_n)]. \quad (3)$$

We computed noise correlation with Eqs 2 and 3 for n = 8 stimulus orientations (both for experimental data and the model).

In addition, for each pair we computed the mean firing rate and the geometric mean defined as:

$$\sqrt{(\overline{FR}_1 \cdot \overline{FR}_2)} \quad (4)$$

In order to remove potential artifacts in the calculation of correlation coefficient, such as slow–wave fluctuations in responses across trials, all the neurons used in the correlation analysis underwent detrending. Therefore the spike counts for each trial were high-pass filtered using a linear–phase Finite Impulse Response (FIR) filter (cf. Bair et al., 2001; Kohn and Smith, 2005).

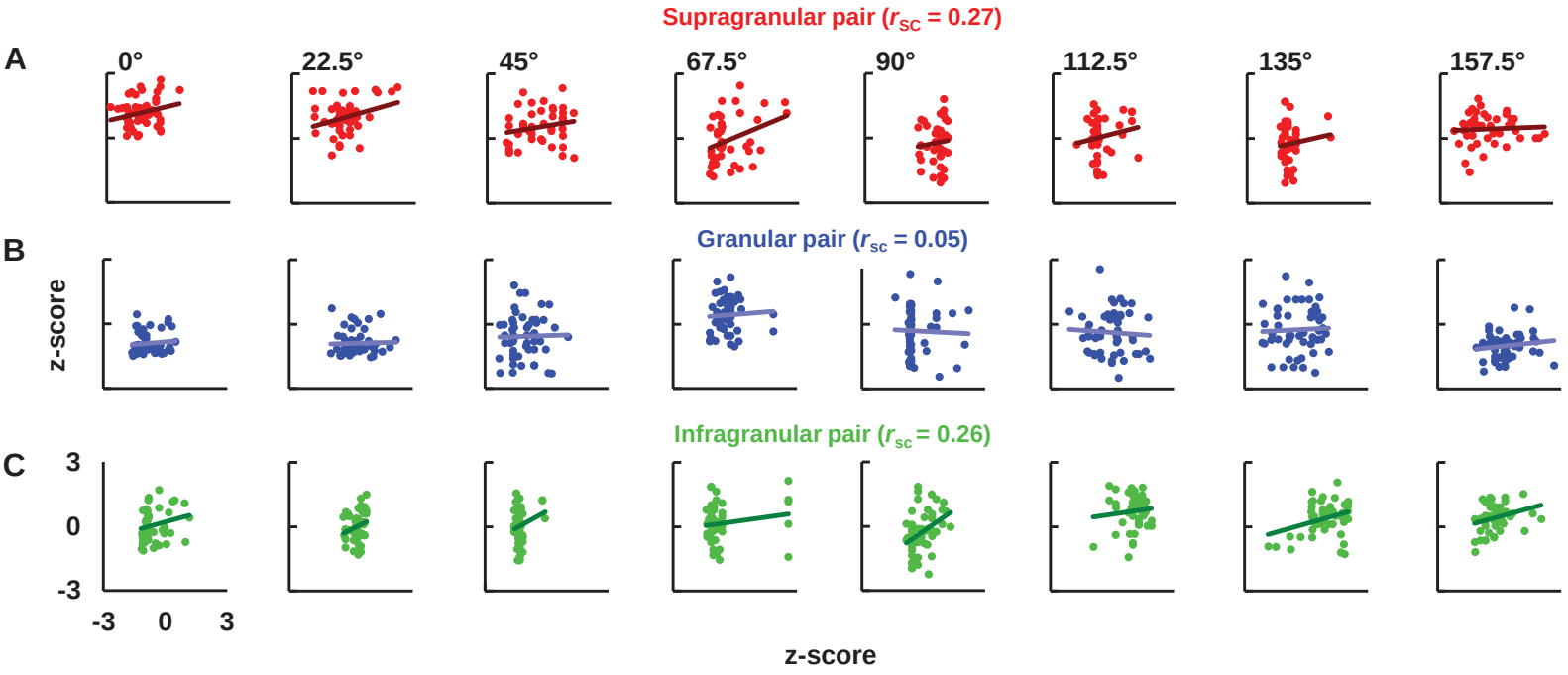

Figure S1. Layer–dependent changes in spike count correlations

(A–C) Each scatter plot represents the z score–transformed responses for pairs of cells recorded simultaneously either in the supragranular (A), granular (B), or infragranular (C) layer during the presentation of a particular stimulus orientation (columns: 0–180° in 22.5° steps). The trend line represents the linear regression fit for each pair of cells; r_{SC} for each layer represents the average noise correlation over n = 8 stimulus orientations (**Experimental Procedures**).

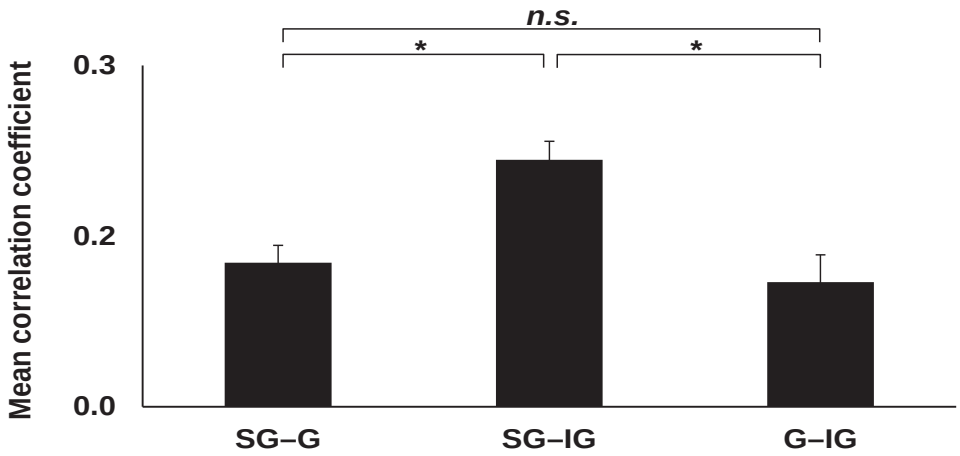

Figure S2. Noise correlation between cortical layers

We calculated noise correlations for neuron pairs originating from different layers and found that correlations between neurons in the granular layer and those in other cortical layers were significantly weaker than those between the supragranular and infragranular layers. When we computed correlations between neurons in supragranular and infragranular layers we observed significantly higher values (SG–IG: 0.21 ± 0.03; one–way ANOVA, F (2, 156) = 12.73, P = 10^{-5}; post–hoc multi–comparison, Tukey's Least Significant Difference). Error bars represent SEM.

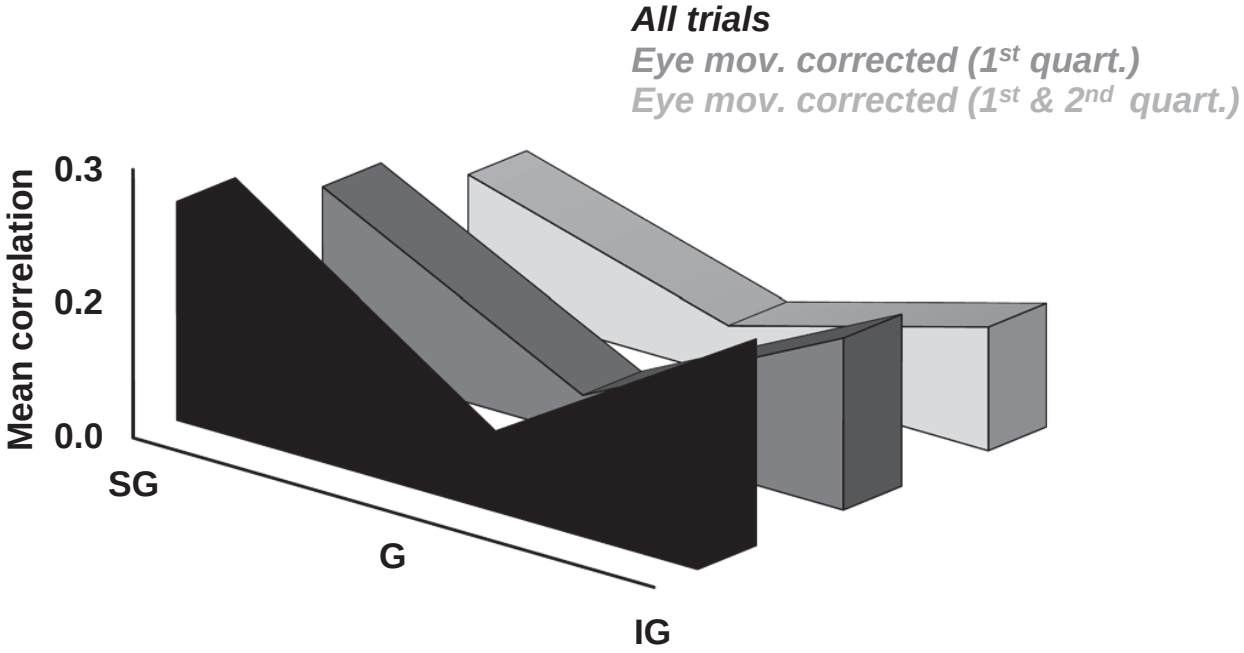

Figure S3. The effect of eye movements on laminar–specific noise correlations
We identified the trial–to–trial changes in microsaccade amplitude and velocity and removed from the calculation of noise correlations the 1st quartile (dark grey) and 1st and 2nd quartile (light grey) trials. The 'all trials' (black) area represents the mean noise correlations from our main experiment (cf. Figure 3A). The grey areas represents the layer–specific mean noise correlation coefficient after removing the 1st quartile microsaccade amplitude and velocity trials (grey; one–way ANOVA, $F(2, 324) = 16.13$, $P = 10^{-7}$), and the layer–specific mean noise correlation coefficient after removing the 1st and 2nd quartiles for microsaccade amplitude and velocity trials (light grey; one–way ANOVA, $F(2, 324) = 7.45$, $P = 0.0007$; post–hoc multi–comparison, Tukey's Least Significant Difference).

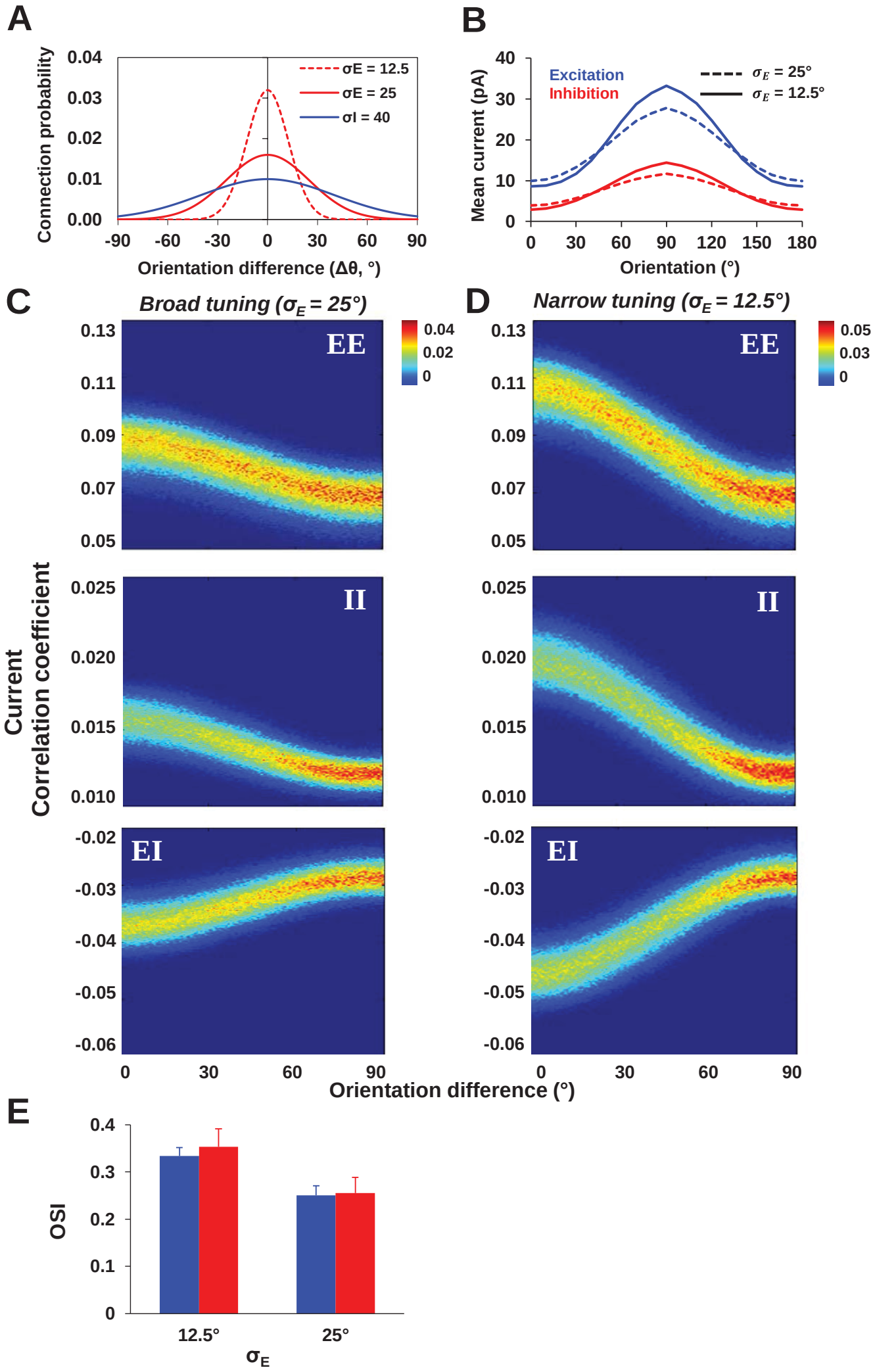
A
Connection probability
0.04
0.03
0.02
0.01
0.00
σE = 12.5
σE = 25
σI = 40
-90
-60
-30
0
30
60
90
Orientation difference (Δθ, °)
B
Mean current (pA)
40
30
20
10
0
Excitation
Inhibition
σ_E = 25°
σ_E = 12.5°
0
30
60
90
120
150
180
Orientation (°)
C
Broad tuning (σ_E = 25°)
D
Narrow tuning (σ_E = 12.5°)
EE
II
EI
0.13
0.11
0.09
0.07
0.05
0.025
0.020
0.015
0.010
-0.02
-0.03
-0.04
-0.05
-0.06
0.04
0.02
0
0.05
0.03
Current
Correlation coefficient
0
30
60
90
Orientation difference (°)
E
OSI
0.4
0.3
0.2
0.1
0
12.5°
25°
σ_E

Figure S4. Single layer model simulations

(A) Neurons were connected randomly according to a normal distribution centered at the 0° difference in the preferred orientation of the cells in a pair (Δθ). The y–axis represents the probability that a postsynaptic neuron receives excitatory and inhibitory input from a cell oriented Δθ degrees away. The inhibitory inputs to a cortical neuron originate from a broader range of orientations than the excitatory inputs. We exemplify the connection probabilities corresponding to broadly tuned excitation ($\sigma_E = 25°$), narrowly tuned excitation ($\sigma_E = 12.5°$), and inhibition ($\sigma_I = 40°$). (B) For each neuron, the mean orientation tuning curves of the excitatory (blue) and inhibitory (red) post–synaptic currents were computed for 18 stimulus orientations separated by 10°, in 50 trials of 0.5 s each. The tuning curves of all neurons were aligned at 90° and then averaged for each synaptic connection profile ($\sigma_E = 25°$; dashed-lines and $\sigma_E = 12.5°$ solid lines). Mean current correlations were computed as the time average of the current correlations for a 250 ms time window. (C) Top, probability distribution of excitatory synaptic current correlations (EE) as a function of the orientation difference between the cells in a pair (Δθ) for broadly tuned ($\sigma_E = 25°$ $\sigma_I = 40°$) excitatory synaptic inputs. (C) Middle, probability distribution of inhibitory synaptic current correlations (II) as a function of the orientation difference between the cells in a pair (Δθ) for broadly tuned excitatory synaptic inputs. (C) Bottom, probability distribution of excitatory–inhibitory synaptic current correlations (EI) as a function of the orientation difference between the cells in a pair (Δθ) for broadly tuned excitatory synaptic inputs. (D) Same as in (C) for sharply tuned ($\sigma_E = 12.5°$ $\sigma_I = 40°$) excitatory synaptic inputs. (E) The orientation tuning of excitatory currents is relatively similar to that of inhibitory currents (measured using the orientation selectivity index, OSI) both for small ($\sigma_E = 12.5°$) and large ($\sigma_E = 25°$) spreads of excitatory connections. Error bars represent standard deviation.

Supplementary methods (modeling)

Integrate-and-fire V1 model

The model has three blocks: ***retina***, ***LGN***, and ***V1***. Retina has analog units driven by the input image. Retinal units activate the LGN units which modulate Poisson spike generators. Subsequently, LGN spikes are sent to the V1 network.

A. Retina

Retina contains two layers of ON-center surround cells, and respectively OFF-center surround cells, driven by image inputs. Each layer has 441 cells arranged in a 21 x 21 array, with spacing between cells of 0.2° of visual angle. Inputs consist of 4 x 1 degree oriented bars presented for 500 ms. Retinal cells are modeled by a difference of Gaussian filters. Retinal activity is modulated by a saturating nonlinearity to account for the stimulus contrast sensitivity, and then the output is sent to the LGN cells with a random delay. The center and surround retinal subfield responses are given by the convolution of the image $I(x,y,t)$ with the corresponding spatial–temporal receptive subfield:

$$R_s(x,y,t) = \int_{-\infty}^{+\infty}\int_{-\infty}^{+\infty}\int_{-\infty}^{t} F_s(x-x',y-y')G_s(t-t')I(x',y',t')dx'dy'dt' \qquad (1)$$

where s = {center, surround}, $F_s(x,y)$ is the spatial term and $G_s(t)$ is the temporal term of the center/surround receptive field. The spatial center/surround fields $F_s(x,y)$ are modeled as circularly symmetric Gaussians, whereas the temporal profiles $G_s(t)$ are modeled as decaying exponentials:

$$F_s(x,y) = \frac{K_s}{2\pi\sigma_s^2}\exp\left(-\frac{x^2+y^2}{2\sigma_s^2}\right)$$
$$G_s(t) = \frac{1}{\tau_s}\exp\left(-\frac{t}{\tau_s}\right) \qquad (2)$$

We used σ_{center} = 0.176°, K_{center} = 17, σ_{surround} = 0.53°, K_{surround} = 16, τ_{center} = 10 ms and τ_{surround} = 20 ms. The stimulus was a rectangular bar of width w = 1°, length l = 4° and contrast c = 100%. The bar was presented for 500 ms, and formed an angle θ with respect to the x–axis. Subfield

responses to a bar of orientation θ centered at the origin (0,0), $R_s(x,y,t|\theta)$, are obtained by rotating the spatial coordinates of the response $R_s(x,y,t|0)$ by θ degrees:

$$R_s(x,y,t\mid\theta) = R_s(x\cos\theta - y\sin\theta, x\sin\theta + y\cos\theta, t\mid 0)$$
$$R_s(x,y,t\mid 0) = g(c)K_s \int_{-w/2}^{w/2}\int_{-l/2}^{l/2} \frac{1}{2\pi\sigma_s^2}\exp\left(-\frac{(x-x')^2+(y-y')^2}{2\sigma_s^2}\right)dx'dy' \int_0^t \frac{1}{\tau_s}\exp\left(\frac{t-t'}{\tau_s}\right)dt' \qquad (3)$$

The effective intensity of the stimulus, $g(c)$, at contrast c, is $g(c) = 3\log_{10}(c)$. This ensures that the contrast dependence of the LGN responses is consistent with experimental data (Somers et al., 1995). The firing rates of ON and OFF retinal ganglion cells are determined by the firing rates of their associated subfields:

$$R_{ON}(x,y,t\mid\theta) = \left[R_{baseline} + R_{center}(x,y,t\mid\theta) - R_{surround}(x,y,t-\delta\mid\theta)\right]^+$$
$$R_{OFF}(x,y,t\mid\theta) = \left[R_{baseline} - R_{center}(x,y,t\mid\theta) + R_{surround}(x,y,t-\delta\mid\theta)\right]^+ \qquad (4)$$

where $[\cdot]^+ = \max(\cdot,0)$ and δ is a 3 ms delay between center and surround field responses. We used $R_{baseline}$ = 15 sp/s as the spontaneous firing rate.

B. LGN

LGN cells are organized in two layers of ON and OFF cells, arranged in arrays of 21 x 21. There is one–to–one correspondence between the retinal cells and LGN cells. The firing rate of ON cells is given by $R_{ON}(x,y,t-\delta_{syn}|\theta)$, and the firing rate of OFF cells is given by $R_{OFF}(x,y,t-\delta_{syn}|\theta)$, where R_{ON} and R_{OFF} are computed with Eq. (4), and δ_{syn} is a random synaptic delay. The synaptic delay has a Gaussian distribution with a mean of 3 ms and standard deviation of 1 ms. These parameters ensures that the peak response of the LGN cells as a function of contrast is well approximated by $R_{LGN}(c) = R_{baseline} + 25\left[\log_{10}(c)\right]^+$.

LGN afferents for each cortical cell are randomly chosen from the arrays of ON and OFF cells (Somers et al., 1995). The probability of a connection between an ON/OFF LGN cell located at position (x,y) and a cortical cell with preferred orientation φ is labeled $P_+(x,y,\varphi)$ (respectively $P_-(x,y,\varphi)$). The connection probability $P_\pm(x,y,\varphi)$ is given by:

$$P_{\pm}(x,y,\phi) = \frac{\left[\pm G(x,y,\phi)\right]^{+}}{\int dxdy\left[\pm G(x,y,\phi)\right]^{+}} \tag{5}$$

$$G(x,y,\phi) = \exp\left(-\frac{x^2}{2\sigma_x^2} - \frac{y^2}{2\sigma_y^2}\right)\cos\left[2\pi f\,(x\cos\phi - y\sin\phi)\right] \tag{6}$$

The positive portions of the Gabor function $G(x,y,\varphi)$ correspond to the ON subfields, and the negative portions correspond to the OFF subfields. We used $\sigma_x = \sigma_y = 0.7$ for the receptive fields and 0.5 cycles per degree for the preferred spatial frequency f. Each excitatory cortical cell received 24 ON and 24 OFF LGN afferents and each inhibitory cortical cell received 16 ON and OFF LGN afferents (all LGN afferents are excitatory). The connections were drawn without replacement from the probability distributions given by equation (5). The connection strengths are given by $|G(x,y,\varphi)|$. Spikes that are sent to the cortical neurons via thalamocortical afferents had a firing rate equal to the output firing rate of the LGN cells modulated by their connection strength to V1. The Poisson spike generator had a refractory period drawn from a uniform process having a mean of 2 ms and standard deviation of 2 ms (Dayan and Abbott, 2001).

We choose the model parameters such as to ensure that the LGN input to a cortical cell is significantly, but broadly, tuned for orientation. The significant orientation tuning of the LGN input to V1 is supported by experimental data (Chung and Ferster, 1998; Ferster, 1986) showing that cortical inactivation does not cause a significant alteration of the width of orientation tuning of the visually evoked EPSPs (the orientation tuning of the inactivated intracortical input to these cells is similar to that of the thalamic input).

C. One-layer cortical network

We implemented a one-layer recurrent cortical model (Somers et al., 1995; Chelaru and Dragoi, 2008) consisting of 1008 excitatory regular spiking and 252 inhibitory fast–spiking cells. The network exhibits 252 preferred orientations in the interval (0^o, 180^o), with 4 excitatory neurons and one inhibitory neuron per orientation. All neurons are modeled as conductance-based, integrate-and-fire neurons. The thalamocortical afferents are established at random from ON and OFF subfields defined over the ON and OFF LGN layers using Gabor functions. Each cortical neuron is modeled as a single compartment with the membrane voltage V_i given by:

$$C_m \frac{dV_i}{dt} = -\sum_j g_{ij}(t-\tau_{ij})(V_i(t)-E_{EXCIT}) - \sum_j g_{ij}(t-\tau_{ij})(V_i(t)-E_{INHIB}) \\ -g_{LEAK}(V_i(t)-E_{LEAK}) - g_{AHP}(t)(V_i(t)-E_{AHP}) \quad (7)$$

The sum over *j* includes only the presynaptic cells that were drawn probabilistically as described below. We used the reversal potentials E_{EXCIT} = 0 mV, E_{INHIB} = -70 mV, E_{LEAK} = -65 mV and E_{AHP} = -90mV. For excitatory (regular spiking) neurons we used: C_m = 0.5 nF, g_{LEAK} = 25 nS and g_{AHP} = 40 nS. For inhibitory (fast spiking) neurons we used: C_m = 0.2 nF, g_{LEAK} = 20 nS and g_{AHP} = 20 nS. Parameters τ_{ij} are synaptic delays. They were chosen from zero bounded normal distributions. Intracortical synapses between excitatory and inhibitory neurons have a mean synaptic delay of 3 ms and 1 ms^2 variance. Thalamocortical synapses onto excitatory and inhibitory neurons had mean synaptic delays of 10 ms and 5 ms, with variances of 5 ms^2 and 3 ms^2, respectively.

The synaptic conductance $g_{ij}(t)$ is given by an alpha–function:

$$g_{ij}(t) = \bar{g}_{ij} \sum_p [t - t_{jp}]^+ \left(\frac{e}{\tau_{peak}} \right) \exp\left(-\frac{t - t_{jp}}{\tau_{peak}} \right) \quad (8)$$

where t_{jp} is the time of the p^{th} spike from the presynaptic cell *j*. Conductances reach their maximum values at τ_{peak}, which is 1 ms for excitatory synapses, 2 ms for inhibitory synapses, and 2 ms for after–hyperpolarization (*AHP*) synapses. The conductances $\bar{g}_{ij}$ represent the maximum conductance changes produced by pre–synaptic spikes. For the synapses afferent to excitatory neurons we used $\bar{g}_{e\_LGN}$ = 2.6 nS, $\bar{g}_{e\_EXCIT}$ = 1.15 nS, $\bar{g}_{e\_INHIB}$ = 4.5 nS and $\bar{g}_{e\_AHP}$ = 40 nS. For the synapses afferent to inhibitory neurons we used $\bar{g}_{i\_LGN}$ = 3 nS, $\bar{g}_{i\_EXCIT}$ = 1.4 nS, $\bar{g}_{i\_INHIB}$ = 5.25 nS and $\bar{g}_{i\_AHP}$ = 20 nS.

Each excitatory neuron has 24 ON and 24 OFF–LGN afferents, 72 synapses from excitatory neurons, and 24 synapses from inhibitory neurons. Each inhibitory neuron has 16 ON and 16 OFF LGN afferents, 56 synapses from excitatory neurons, and 16 synapses from inhibitory neurons. LGN synapses are excitatory, and the pre–synaptic cell positions and synaptic strengths

were defined using Gabor functions (see above). Each cortical neuron has a network position identified by its preferred orientation.

For each cortical neuron, the excitatory and inhibitory pre–synaptic neuron positions were drawn from a normal distribution with mean value at the neuron's preferred orientation and the same standard deviations σ_E and σ_I for excitatory and inhibitory synapses. The standard deviation of the distribution of connection probability for excitatory neurons was varied in steps of 10° in the [10°, 60°] range to allow the investigation of the relationship between the spatial spread of excitatory connections and the magnitude of noise correlations (**Figure 5**E).

When membrane potential exceeded the baseline spike threshold of -55 mV, a spike was generated and the *AHP* conductance was activated. After spike generation, during an absolute refractory period (3 ms for excitatory and 1.5 ms for inhibitory neurons), spike generation was aborted. After a spike is emitted, the relative refractory periods are generated by elevating the spike threshold by 10 mV and then decreasing it to -55 mV (baseline) with a 10 ms time constant (cf. Somers et al., 1995). Neuronal differential equations were numerically integrated with a fixed step fourth order Runge–Kutta method. Integration step was 0.5 ms. For each excitatory neuron, excitatory and inhibitory synaptic currents were computed as sums of the corresponding pre-synaptic currents, sampled every 2 integration steps (1 KHz).

D. Three-layer cortical network

We implemented three coupled recurrent networks of excitatory and inhibitory neurons that modeled the supragranular layers 2/3, granular layer 4, and infragranular layers 5/6. The retina and LGN networks are similar to those described in sections A and B. Each laminar network consists of 504 excitatory and 126 inhibitory neurons. Each cortical neuron is modeled as a single compartment with the membrane voltage given by equation (7). The reversal potentials, C_m, g_{LEAK}, and g_{AHP} in equation (7) are similar to those in section C. However, we modified the number of synapses and synaptic conductances to model the intra-layer connectivity and scale each network from 1008 to 504 excitatory neurons and from 252 to 126 inhibitory neurons respectively. Thus, each excitatory neuron in the granular layer received 24 LGN inputs, 12 inputs from infragranular layer, and 36 excitatory and 12 inhibitory inputs from nearby neurons

in the same layer. For afferent synapses we used $\overline{g}_{e\_LGN}$ = 4 nS, $\overline{g}_{e\_EXCIT}$ = 2.3 nS and $\overline{g}_{e\_INHIB}$ = 8.5 nS in equation (8). For synapses from the infragranular layer we used $\overline{g}_{e\_CORT}$ = 2.3 nS. Each inhibitory neuron in the granular layer received 12 LGN inputs, 9 inputs from the infragranular layer, and 28 local excitatory and 8 local inhibitory inputs. For afferent synapses we used $\overline{g}_{i\_LGN}$ = 6 nS, $\overline{g}_{i\_CORT}$ = 2.8 nS, $\overline{g}_{i\_EXCIT}$ = 2.8 nS and $\overline{g}_{i\_INHIB}$ = 10.5 nS.

Synaptic connectivities were defined as in the case of the one-layer network using Gaussian distributions. For both local and external excitatory inputs we used a distribution of $\sigma_E = 30°$, while for the inhibitory inputs we used $\sigma_I = 40°$, both for excitatory and inhibitory neurons in the granular layer. Intracortical synapses between excitatory and inhibitory neurons had a mean synaptic delay of 2 ms and 1 ms^2 variance, while feedforward synapses connecting infragranular and granular layer neurons (both excitatory and inhibitory) had a mean synaptic delay of 3 ms and 1 ms variance to account for spike delay transmission (Rasch et al., 2011).

Each supragranular excitatory neuron received 24 inputs from the granular layer and 36 local excitatory and 12 local inhibitory inputs. Each inhibitory neuron received 16 excitatory inputs from the granular layer and 28 local excitatory and 8 local inhibitory inputs. Infragranular excitatory and inhibitory neurons had the same structure of synaptic inputs as those in supragranular layer (except that feedforward inputs arrive from supragranular layers). For both supragranular and infragranular layers we used a distribution of $\sigma_E = 15°$ for local excitatory inputs, $\sigma_E = 20°$ for external excitatory inputs, and $\sigma_I = 40°$ for local inhibitory inputs. Intracortical synapses between excitatory and inhibitory neurons had a mean synaptic delay of 2 ms and 1 ms^2 variance. Synapses connecting granular and supragranular layer neurons had a mean synaptic delay of 3 ms and 1 ms^2 variance; synapses connecting supragranular and infragranular layer neurons had a mean synaptic delay of 4 ms and 1 ms^2 variance to account for spike delay transmission (Rasch et al., 2011).

The structure of synaptic connectivity within and between layers ensured model mean noise correlations in the (0°, 30°) orientation range that matched experimental data for each cortical layer (**Figure 6**B). Orientation discrimination performance for each layer network was estimated

using Fisher information from the spike counts in each layer obtained when bar stimuli of two nearby orientations (90° and 92°) were presented for 504 trials of 0.5 sec duration (**Figure 6**B).

Spike count and current correlations

Spike count (noise) correlations were computed by averaging the correlations of net response to six different orientations of the bar stimulus, separated by 30°, in the interval [0°, 150°] (see **Experimental Procedures**, Eq. 2 and Eq. 3). Current correlation between the synaptic currents of any two neurons *i* and *j* was computed by averaging over trials the area under the cross-correlation of synaptic currents for an interval of 250 ms (**Figure S4**C-D).

Network orientation discrimination threshold

For a population of *N* neurons characterized by orientation tuning curves $\boldsymbol{f}(\theta) = \{ f_1(\theta), f_2(\theta), \ldots, f_N(\theta)\}$ and a multivariate Gaussian trial–to–trial variability of the population response defined by the covariance matrix $\boldsymbol{Q}(\theta)$, Fisher Information (FI) stimulus orientation θ is computed as:

$$FI(\theta) = \boldsymbol{f}'(\theta)^{T}\boldsymbol{Q}^{-1}(\theta)\,\boldsymbol{f}'(\theta) + 0.5\mathrm{Tr}[\boldsymbol{Q}'(\theta)\,\boldsymbol{Q}^{-1}(\theta)\,\boldsymbol{Q}'(\theta)\,\boldsymbol{Q}^{-1}(\theta)] \qquad (9)$$

where $\boldsymbol{f}'(\theta)$ and $\boldsymbol{Q}'(\theta)$ are the derivative of the tuning curves and covariance matrix respectively (Abbott and Dayan, 1999). For larger neuronal populations, the direct FI computation with equation (9) may be practically impossible because of numerical difficulties associated with inverting large covariance matrices, and therefore the direct calculation of FI is usually replaced by an estimation of FI based on various decoders, such as the linear locally optimal estimator (Seriès et al. 2004; Chelaru and Dragoi, 2008). We used a linear decoder that estimated stimulus orientation θ from the firing rates of excitatory neurons as:

$$\hat{\theta} = W^{T}R + b \qquad (10)$$

where *W* is a weight vector, *b* is a scalar and *R* is the firing rate of the excitatory neurons. Linear decoders allow the estimation of the first term of FI from equation (9) as:

$$I_{LD} = \frac{\left(\left(\left\langle\hat{\theta}_2\right\rangle - \left\langle\hat{\theta}_1\right\rangle\right)/\Delta\theta\right)^2}{\sqrt{\sigma^2_{\hat{\theta}_2} + \sigma^2_{\hat{\theta}_1}}} \qquad (11)$$

where $\Delta\theta = \theta_2 - \theta_1$, $\left\langle \hat{\theta}_i \right\rangle$ is the mean, and $\sigma^2_{\hat{\theta}_i}$ (i = 1,2) is the variance of the linear decoder output when a bar stimulus of orientation θ_i is presented to the retina (Series et al., 2004).

Decoder weights W and b were optimized such as to minimize the discrimination threshold between two nearby stimulus orientations, θ_1 and θ_2 (we used θ_1=90° and θ_2=92°). We used as discrimination threshold the upper bound $\Delta\theta_{TH}$ of the change in orientation, $\Delta\theta$, which can be detected 75% of the trials by an ideal observer (Green and Swets, 1966), related to the estimate I_{LD} of the FI through:

$$\Delta\theta_{TH} = \frac{1.35}{\sqrt{I_{LD}}} \tag{12}$$

The discrimination threshold $\Delta\theta_{TH}$ was minimized by computing the decoder weights W and b such as information I_{LD} was maximized. First, we generated 504 trials in which a bar of orientation θ_1 was presented, followed by 504 trials in which a bar of orientation $\theta_2 = \theta_1 + \Delta\theta$ was presented. Each stimulus was presented for 500 ms. We trained three linear decoders, one for each layer, such as to minimize the discrimination threshold $\Delta\theta_{TH}$ of each layer. In order to train each linear decoder we divided the responses of corresponding layer into equal sets: a training set and a test set. We used the training set (252 trials with orientation θ_1 and 252 trials with orientation θ_2) to compute the linear decoder weights (Eq. 10) by using the conjugate gradient algorithm (Hagan et al., 1966). For each of the algorithm iterations, we computed information I_{LD} from equation (11) using the test set and decoder weights computed in that iteration. We used a number of 504 iterations, equal to the dimension of the linear decoder (defined by the number of excitatory neurons in each layer; the minimum of the surface error for a linear decoder trained using the conjugate gradient algorithm is reached at most after a number of iterations equal to decoder dimension). We kept the weights of the decoder corresponding to the maximum I_{LD}, and then computed the mean network discrimination threshold $\Delta\theta_{TH}$ from five experimental sessions (**Figure 6**B).

SUPPLEMENTAL REFERENCES

Bair, W., Zohary, E., and Newsome, W.T. (2001). Correlated firing in macaque visual area MT: time scales and relationship to behavior. J Neurosci 21, 1676-1697.

Chung, S., and Ferster, D. (1998). Strength and orientation tuning of the thalamic input to simple cells revealed by electrically evoked cortical suppression. Neuron 20, 1177-1189.

Dayan, P., and Abbott, L.F. (2001). Theoretical Neuroscience (Cambridge: The MIT Press).

Dragoi, V., Rivadulla, C., and Sur, M. (2001). Foci of orientation plasticity in visual cortex. Nature 411, 80-86.

Dragoi, V., Sharma, J., Miller, E.K., and Sur, M. (2002). Dynamics of neuronal sensitivity in visual cortex and local feature discrimination. Nat Neurosci 5, 883-891.

Dragoi, V., Sharma, J., and Sur, M. (2000). Adaptation-induced plasticity of orientation tuning in adult visual cortex. Neuron 28, 287-298.

Ferster, D. (1986). Orientation selectivity of synaptic potentials in neurons of cat primary visual cortex. J Neurosci 6, 1284-1301.

Hansen, B.J., Eagleman, S., and Dragoi, V. (2011). Examining local network processing using multi-contact laminar electrode recording. J Vis Exp.

Green, D.M., and Swets, J.A. (1966). Signal detection and psychophysics (New York: Wiley).

Gutnisky, D.A., and Dragoi, V. (2008). Adaptive coding of visual information in neural populations. Nature 452, 220-224.

Hagan, M., Demuth, H., and Beale, M. (1966). Neural Network Design (Boston: PWS Publishing).

Pettersen, K.H., Devor, A., Ulbert, I., Dale, A.M., and Einevoll, G.T. (2006). Current-source density estimation based on inversion of electrostatic forward solution: effects of finite extent of neuronal activity and conductivity discontinuities. J Neurosci Methods *154*, 116-133.

Rasch, M.J., Schuch, K., Logothetis, N.K., Maass, W. (2011). Statistical Comparison of Spike Responses to Natural Stimuli in Monkey Area V1 with Simulated Responses of a Detailed Laminar Network Model for a Patch of V1, J Neurophysiol 105, 757-778.

Series, P., Latham, P.E., and Pouget, A. (2004). Tuning curve sharpening for orientation selectivity: coding efficiency and the impact of correlations. Nat Neurosci 7, 1129-1135.

Somers, D.C., Nelson, S.B., and Sur, M. (1995). An emergent model of orientation selectivity in cat visual cortical simple cells. J Neurosci 15, 5448-5465.